Analysis of regular and irregular acoustic streaming patterns in a rectangular enclosure

Majid Nabavi [a,b,*], Kamran Siddiqui [a,c], Javad Dargahi [a]

[a] Department of Mechanical and Industrial Engineering, Concordia University, Montreal, Quebec, Canada
[b] Department of Mechanical Engineering, McGill University, Montreal, Quebec, Canada
[c] Department of Mechanical and Materials Engineering, University of Western Ontario, London, Ontario, Canada

ARTICLE INFO

ABSTRACT

This study reports an experimental investigation of the non-linear phenomena of regular (classical) and irregular streaming patterns generated in an air-filled rigid-walled square channel subjected to the acoustic standing waves of different frequencies and intensities. The interaction of acoustic waves and thermoviscous fluids is responsible for these phenomena. The resonator's walls are maintained at isothermal condition. Synchronized particle image velocimetry (PIV) technique has been used to measure the streaming velocity fields. The experimental results show that at a given excitation frequency, regular streaming flow patterns are observed up to a certain value of the excitation amplitude. As the amplitude increases beyond this limit, the regular streaming is distorted to an irregular flow structure. The regular and irregular streaming are classified in terms of streaming Reynolds number $\left(Re_{s2} = \frac{1}{2}(u_{max}/c)^2 (H/\delta_v)^2\right)$. It is found that for $Re_{s2} < 50$, classical streaming flow patterns are established and then deform to irregular and complex shapes as Re_{s2} exceeds 50.

© 2009 Published by Elsevier B.V.

1. Introduction

It is a well-known fact that the motion of the fluid particles in a sound field or in the adjacent boundary layers of oscillating boundaries generates a time-independent motion of the fluid particles which is called *acoustic streaming* [1]. Acoustic streaming is an important non-linear phenomenon caused by the interaction of acoustic waves in thermoviscous fluids and solid boundaries. One type of the acoustic streaming which is always associated with a standing-wave resonator is called Rayleigh or outer streaming. Rayleigh streaming is a vortex-like structure outside the boundary layer generated by and superimposed on the acoustic standing wave in a closed enclosure. Vortex motion generated inside the boundary layer is called Schlichting or inner streaming [2].

The acoustic streaming flow patterns can be categorized into regular and irregular streaming. The regular streaming appears as two streaming vortices per quarter-wavelength of the acoustic wave which are symmetric about the channel center line. In irregular streaming, the shape and number of the streaming vortices are different from the regular case. The regular and irregular acoustic streaming patterns have been extensively investigated both analytically and numerically. In order to analyze acoustic streaming formation, the general Navier–Stokes and energy equations should be solved using appropriate analytical or numerical methods [3,4]. By using successive approximations, Kildal [5] studied the time-dependent as well as the time-independent fluid motion above a vibrating plate. Carlsson et al. [6] performed an analytical study of the steady

* Corresponding author. Address: Department of Mechanical and Industrial Engineering, Concordia University, Montreal, Quebec, Canada. Tel.: +1 514 8482424x7102; fax: +1 514 8483175.

E-mail address: m_nabav@encs.concordia.ca (M. Nabavi).

streaming flow induced by vibrating solid walls and argued that both vibrational frequency and normalized channel width affect the streaming flow. Kawahashi and Arakawa [7] developed a two-dimensional numerical model for the acoustic streaming induced by finite amplitude oscillation of an air-column in a closed duct and concluded that the structure of acoustic streaming changes with the oscillation amplitude. They found that when the amplitude is sufficiently large, circulatory streaming develops which is then distorted to a complicated and irregular flow structure at very large oscillation amplitudes. The distortion of acoustic streaming pattern due to the fluid inertia at relatively large acoustic amplitudes has been observed using numerical analysis by Menguy and Gilbert [8]. They showed that at large oscillation amplitudes, the effect of fluid inertia on the streaming must be taken into account. Aktas and Farouk [9] simulated the acoustic streaming motion in a compressible gas-filled two-dimensional rectangular enclosure and numerically investigated the effects of sound field intensity on the formation process of streaming flow structures. They found that up to a certain value of the enclosure height to wavelength ratio, the vibrational motion causes classical and steady streaming flows. However, when the enclosure height is increased beyond this limit, the streaming flow structures become irregular and complex.

While many papers can be found about the analytical and numerical methods to analyze acoustic streaming, relatively few experimental investigations have been performed to measure the two-dimensional acoustic streaming velocity fields inside a standing-wave resonator. This scarceness is due to the lack of appropriate techniques to resolve the streaming velocity which is imposed on the large magnitude acoustic velocity. The acoustic velocity is typically one or two order of magnitude higher than the corresponding streaming velocity. That is why all of the reported measurements of streaming velocity fields have been performed in the vicinity of a velocity node, where the amplitude of the acoustic velocity is almost zero [10,11]. Thompson et al. [12,13] used laser Doppler anemometry (LDA) to study the acoustic streaming generated in a cylindrical standing-wave resonator filled with air. They observed that as the excitation amplitude increases, the difference between the experimental and theoretical acoustic velocities increases due to the fluid inertial effect. Moreau et al. [14] have used LDA to measure inner and outer streaming vortices at different streaming Reynolds numbers and different frequencies (f = 88, 113 and 150 Hz). They observed that for high values of streaming Reynolds number, the axial streaming velocity starts to depart from the theoretical slow streaming. It should be noted that their experiments have been performed at uncontrolled thermal boundary conditions. The LDA measures velocity at one spatial location at a time and therefore, is not capable of simultaneously mapping the flow in a two-dimensional region. Recently, the authors have developed a novel approach using synchronized particle image velocimetry (PIV) technique to simultaneously measure two-dimensional acoustic and streaming velocity fields at different spatial locations along a resonator and at any wave phase [15]. The authors have then used this technique to investigate the non-linear acoustic velocity fields [16], the onset of acoustic streaming [17], and the influence of differentially heated horizontal walls on the streaming shape and velocity in a standing-wave resonator [18], as well as different flow patterns inside the acoustic standing wave pump [19].

In the present study, we have used a modified version of the approach reported in [15] to resolve the streaming velocity fields of different magnitudes in presence of acoustic velocity and analyzed the formation of regular and irregular acoustic streaming at different acoustic frequencies and intensities. To the best of authors' knowledge, this is the first two-dimensional experimental investigation of the non-linear phenomena of regular and irregular acoustic streaming inside a standing-wave resonator.

2. Theory

The amplitude of the axial component of the acoustic velocity in the linear case is given as $u = u_{max} \sin(2\pi x/\lambda)$, where x is the axial coordinate and λ is the wavelength. Based on the analytical formula derived by Rott [20], the axial component of the streaming velocity is,

$$u_{st} = (1 + \alpha)\frac{3}{8}\frac{u_{max}^2}{c}\left(1 - \frac{2y^2}{(H/2)^2}\right)\sin(\pi x/l), \tag{1}$$

where c is the sound speed, y is the transverse coordinate ($-H/2 \leqslant y \leqslant H/2$), H is the tube width, and $l = \lambda/4$. In Eq. (1), α is given by $\alpha = \frac{2}{3}(1 - \beta)(\gamma - 1)\frac{\sqrt{Pr}}{1 + Pr}$, where $Pr = v/\kappa$ is the Prandtl number, v is the kinematic shear viscosity, κ is the coefficient of thermal conduction, β is a constant that depends on the properties of the fluid, and γ is the ratio of the specific heat at constant pressure and constant volume. Typical value of α in air is 0.03 which is based on $\gamma = 1.4$, $Pr = 0.71$ and $\beta = 0.77$.

It is useful to discuss some dimensionless parameters which are frequently used in the study of steady streaming flows. The Reynolds number is the ratio of the inertial force to the viscous force and defined as $L_s U_s / v$, where L_s and U_s are the characteristic length and velocity, respectively. Assuming L_s to be the length of the tube and U_s to be the maximum acoustic velocity (u_{max}), the acoustic Reynolds number is defined as

$$Re_a = u_{max}c/v\omega, \tag{2}$$

where $\omega = 2\pi f$, and f is the excitation frequency. Choosing L_s as the width of the tube and U_s as the maximum streaming velocity (which is proportional to u_{max}^2/c), the streaming Reynolds number is defined as

$$Re_{s1} = u_{max}^2/v\omega, \tag{3}$$

One important dimensionless number in streaming studies is the ratio of tube width to viscous boundary layer thickness ($\delta_v = \sqrt{2v/\omega}$). Another definition of the streaming Reynolds number that includes this ratio is,

$$Re_{s2} = \frac{1}{2}\left(\frac{u_{max}}{c}\right)^2\left(\frac{H}{\delta_v}\right)^2, \tag{4}$$

$Re_{s2} \ll 1$ corresponds to the relatively *slow streaming*, whereas $Re_{s2} \gg 1$ is referred to as non-linear streaming [13]. Aktas and Farouk [9] have used Re_{s1} in their numerical study of acoustic streaming. Thompson et al. [12,13] and Menguy and Gilbert [8] have used Re_{s2} in their acoustic streaming analysis.

3. Synchronized PIV technique

In the PIV technique, positions of the flow-tracing particles are recorded at two known times by illuminating the particles using a laser light sheet. A CCD camera captures the images of the particles at each pulse in the flow field of interest. The displacement of particles between the two images divided by the time separation between the laser pulses provides the velocity field. In the conventional PIV setup, the laser pulses are synchronized with the camera frames. Typically these signals are not synchronized with any flow characteristics, as for steady flows it is not necessary. However, for velocity measurements in the presence of acoustic standing wave, two laser pulses and the camera triggering need to be synchronized with the excitation signal to capture the velocity fields at the right phase. The authors have developed a novel approach using synchronized PIV to measure two-dimensional streaming velocity fields, in the presence of acoustic standing wave of different frequencies and intensities [15]. The basic principal of this scheme is shown in Fig. 1. Consider the image taken at time t_1 in Fig. 1 as the first image and the image taken at time t_2 as the second image, with the time separation of $t_2 - t_1$. The cross-correlation of this image pair provides the acoustic velocity field at time t_1. Now, consider the image taken at time t_1 as the first image and the image taken at time t_3 as the second image, with the time separation of $t_3 - t_1$. Since the images acquired at t_1 and t_3 are exactly at the same phase, the acoustic velocity components at these times are equal, therefore, the particle shifts between these two images are only be due to streaming velocity. Thus, the cross-correlation of this image pair provides the streaming velocity field at time t_1 [15].

In the approach reported in [15], the separation time between two images utilized for the streaming velocity measurement ($\delta t = t_3 - t_1$ in Fig. 1) is fixed and equal to 2/*frame rate*. However, to resolve the streaming velocity fields of higher magnitudes and gradients, this value of δt could be too large and may result in large errors. In some cases where the streaming velocity fields are highly rotational or the velocity gradients are very high, the shape and amplitude of the streaming patterns cannot be correctly captured by having a large separation time.

In the present study, as shown in Fig. 2, the separation time is chosen to be an integer multiple of the wave period (T), that is, $\delta t = nT$, $n = 1, 2, \ldots, N$. (N should be chosen so that $1/nT \leqslant$ frame rate of the CCD camera). The appropriate value of n should be determined for each experiment based on the maximum amplitude and gradient of the streaming velocity. For example for the excitation frequency of $f = 1000$ Hz ($T = 1$ ms) and camera frame rate of 30 fps, n can be varied from 1 to 33 depending on the excitation amplitude. for very high amplitude or gradient streaming flows, a small number should be chosen for n to correctly capture the streaming patterns, while for slow streaming flows, a large number should be chosen for n to reduce the error. In the modified synchronized PIV, the time separation between two laser pulses is less than the exposure time of CCD (1/30 s). However, as shown in Fig. 2, the first laser pulse fires near the end of first camera frame and the second lase pulse fires shortly after the beginning of the second camera frame.

The modified synchronized PIV technique allows to measure the streaming flows of different magnitudes and gradients. It should be noted that in this configuration, the synchronized technique cannot measure the acoustic and streaming velocity fields simultaneously. Since the present study is focused on the streaming flows, measurement of the acoustic velocity is not needed.
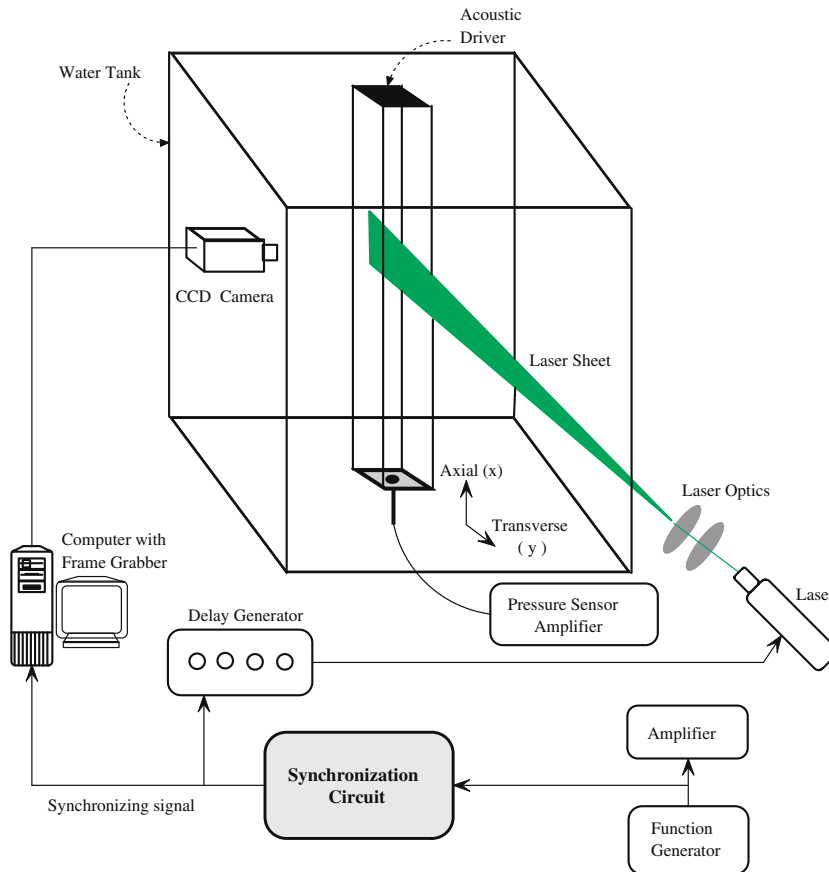
4. Experimental setup

The experimental setup developed to measure the streaming velocity fields inside the standing wave tube is shown in Fig. 3. The acoustic chamber is a Plexiglas channel of square cross-section. The channel is 105 cm long with the inner
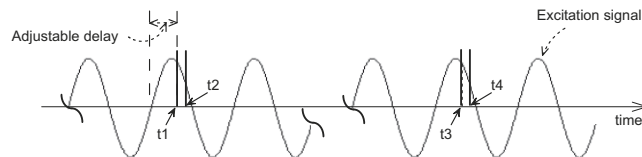
Fig. 1. The triggering sequence that shows the simultaneous measurement of the acoustic and streaming velocity fields at a particular phase of the excitation signal. t_1 and t_2 correspond to the times at which the first and second images of an image pair are captured. t_3 and t_4 are the times associated with the first and second images of the consecutive image pair.
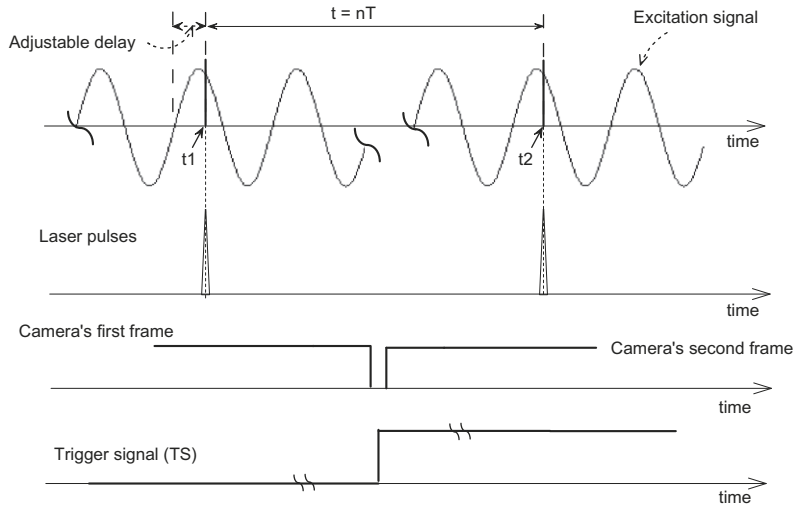
Fig. 2. The triggering sequence that shows the measurement of the streaming velocity field at a particular phase of the excitation signal. t_1 and t_2 correspond to the times at which the first and second images of an image pair are captured.

Fig. 3. Schematic of the experimental setup and instrumentation.

cross-section of 4 cm × 4 cm. The walls of the channel are 10 mm thick, therefore, the assumption of rigid walls held for this channel. The two-dimensional velocity fields inside the channel are measured using synchronized PIV. A 120 mJ Nd:YAG laser is used as a light source for the PIV measurements. A digital two Megapixel progressive scan CCD camera (JAI CV-M2)

with the resolution of 1600×1200 pixels is used to image the flow. The camera is connected to a PC equipped with a frame grabber (DVR Express) that acquired 8 bit images at a rate of 30 Hz. A four-channel digital delay generator (BNC-555-4C) is used to control the timing of the laser pulses. BIS(2-ETHYLHEXYL) SEBACATE mist with the mean diameter of 0.5 μm is used as the tracer particles. An aerosol generator (Lavision Inc.) is used to generate the mist. The acoustic pressure is measured by a condenser microphone cartridge Model 377A10 PCB Piezotronics. The microphone consists of a microphone cartridge and a microphone preamplifier. A preamplifier Model 426B03 is used in order to measure the sound pressure level. The frequency response is almost flat between 5 Hz and 100 kHz. During velocity measurements, the microphone is placed inside a hole at the end wall of the channel (see Fig. 3). Thus, the microphone measured the maximum pressure fluctuation. A special loud-speaker driver is used to excite the acoustic standing wave inside the tube. The driver has the maximum power of 200 W. A Function generator (Agilent 33120A) is used to generate the sinusoidal wave. The accuracy of the generated frequency and amplitude are 1 μHz and 0.1 mV, respectively. The signal from the function generator is amplified by a 220-W amplifier (Pioneer SA-1270). The loudspeaker is driven by this amplified signal (see Fig. 3).

The resonator is filled with air ($c = 344$ m/s, $\rho = 1.2$ kg/m^3). As shown in Fig. 3, the resonator is placed inside a large water tank of $50 \times 50 \times 90$ cm dimensions, in order to completely isolate the resonator from the temperature gradients within the laboratory that can cause ambient convection velocities and affect the streaming patterns. The water temperature is $T = 22.5$ °C. This allows to maintain isothermal boundary condition at the channel walls. The maximum vibrational displacement of the acoustic driver is also measured for each excitation amplitude and frequency. A Brüel & Kjær laser vibrometer is used to measure this parameter.

The characteristic response time of the seed particles is computed by $T_p = u_T/g$, where T_p is the particle response time, u_T is the particle terminal velocity and g is the acceleration due to gravity [21]. The terminal velocity is computed by $u_T = (\gamma - 1)D^2 g/18\nu$, where D is the diameter of the tracer particles [22]. Using the above equations, for $D = 0.5$ μm and $u_T = 6.5$ μm/s, the particle response time is found to be $T_p = 0.67$ μs. For the driver frequency of 1000 Hz, the particle response is more than 1500 times faster than the wave period. Thus, we conclude that the tracer particles accurately follow the flow.

For PIV cross-correlation, the size of the interrogation region is set equal to 32×32 pixels and the size of the search region is set equal to 64×64 pixels. A 50% window overlap is used in order to increase the nominal resolution of the velocity field to 16×16 pixels. A three-point Gaussian sub-pixel fit scheme is used to obtain the correlation peak with sub-pixel accuracy. For each set of measurements, 100 PIV images are captured. From these images, 50 streaming velocity fields are computed using the technique described in Section 3. The spurious velocity vectors are detected and then corrected using a local median test [23].

5. Results and discussion

In this study, three different excitation frequencies (f) and four different maximum vibrational displacements (X_{max}) of the acoustic driver for each frequency are considered. That is, a total of 12 different cases, which are summarized in Table 1. The half-wavelength of the acoustic standing wave (ℓ), normalized channel width (H/ℓ) and normalized maximum vibrational displacement (X_{max}/ℓ) are also listed in Table 1.

In cases A-1–A-4, the frequency of acoustic driver is set equal to 976 Hz ($T = 1.02$ ms). This results in the formation of three full standing waves inside the channel. The field of view of the camera is set equal to 10.3 cm in horizontal and 8 cm in vertical to map the flow field in the quarter-wavelength section of the channel. The separation time between two PIV images of the image pair is set equal to 30 times the wave period (i.e. $\delta t = 30.7$ ms). Cases A-1–A-4, correspond to the maximum vibrational displacement of the acoustic driver (X_{max}) equal to 120 μm, 143 μm, 235 μm and 350 μm, respectively. The corresponding maximum pressure amplitudes (P_0) are 1437, 1780, 2844 and 4375 Pa. All measurements of the

Table 1
The cases considered for the acoustic streaming experiments along with the details of parameters for each case. f, frequency; ℓ, half-wavelength; H/ℓ, normalized channel width; X_{max}, maximum vibrational displacement of the driver.

Case	f (Hz)	$\ell = \lambda/2$ (cm)	H/ℓ	X_{max}(μm)	X_{max}/ℓ
A-1	976	17.6	0.23	120	6.81×10^{-4}
A-2	976	17.6	0.23	143	8.11×10^{-4}
A-3	976	17.6	0.23	235	1.33×10^{-3}
A-4	976	17.6	0.23	350	1.99×10^{-3}
B-1	666	25.8	0.15	510	1.97×10^{-3}
B-2	666	25.8	0.15	640	2.48×10^{-3}
B-3	666	25.8	0.15	850	3.29×10^{-3}
B-4	666	25.8	0.15	1040	4.03×10^{-3}
C-1	1310	13.1	0.3	80	6.09×10^{-4}
C-2	1310	13.1	0.3	102	7.77×10^{-4}
C-3	1310	13.1	0.3	145	1.10×10^{-3}
C-4	1310	13.1	0.3	190	1.45×10^{-3}

streaming flow patterns at each particular excitation amplitude are found to be consistent and steady-state. This allows to average all 50 streaming velocity fields at each particular amplitude for better suppression of the noise.

The time-averaged streaming flow patterns for cases A-1–A-4 are shown in Fig. 4a–d, respectively. The sequence shows the impact of excitation amplitude on the structure of the streaming flow as it increases from case A-1 to case A-4. The plot in Fig. 4a shows that at smaller excitation amplitude (case A-1), two streaming vortices per quarter-wavelength are observed which are symmetric about the center line of the channel. This verifies the establishment of the classical streaming flow structure for case A-1. For case A-2, the plot in Fig. 4b shows that the streaming vortices can still be considered as classical streaming. At a higher excitation magnitude (Fig. 4c, case A-3), the irregularity in the shape of the vortices is clearly observed and classical streaming no longer exists for this case. At a higher excitation magnitude (Fig. 4d, case A-4), two additional small vortices are generated at the channel centerline on the left-hand side of the two primary vortices which indicates the formation of irregular streaming patterns.

Aktas and Farouk [9] argued that the maximum vibrational displacement of the acoustic driver plays an important role in the formation of regular and irregular streaming flow structures. They predicted that up to a certain value of the vibrational displacement, classical and steady streaming flows are established in the acoustic resonator. However, when the vibrational displacement is increased beyond this limit, the streaming flow structures become irregular and complex. The present results confirm this by showing that the maximum vibrational displacement of the driver has a significant influence on the streaming flow patterns.

In the next set of experimens, the frequency of the acoustic driver is set equal to 666 Hz ($T = 1.5$ ms). The half-wavelength (ℓ) of the acoustic standing wave corresponding to this frequency is 25.8 cm. It allows the formation of two full standing waves inside the channel. The field of view of the CCD camera is set in a way to map the flow field in the quarter-wavelength section of the channel. That is, the field of view of the camera is set equal to 13.1 cm in horizontal and 9.8 cm in vertical. The separation time between two PIV images of the image pair is set equal to 20 times the wave period (i.e. $\delta t = 30.3$ ms). The maximum vibrational displacement (X_{max}) is 510 µm, 640 µm, 850 µm and 1040 µm, for cases B-1–B-4, respectively. The corresponding maximum pressure amplitudes (P_0) are 2469, 3094, 3844 and 4844 Pa.

Fig. 5 depicts the time-averaged streaming velocity fields for these four cases. The plot in Fig. 5a shows that the classical streaming flow structure, i.e. two symmetric vortices in quarter-wavelength is clearly observed for case B-1. As the excitation magnitude increases (Fig. 5b, case B-2), the circular shape of the vortices starts to degrade and cannot be assumed as classical streaming. At further higher excitation magnitudes (cases B-3 and B-4, Fig. 5c and d), additional small vortices
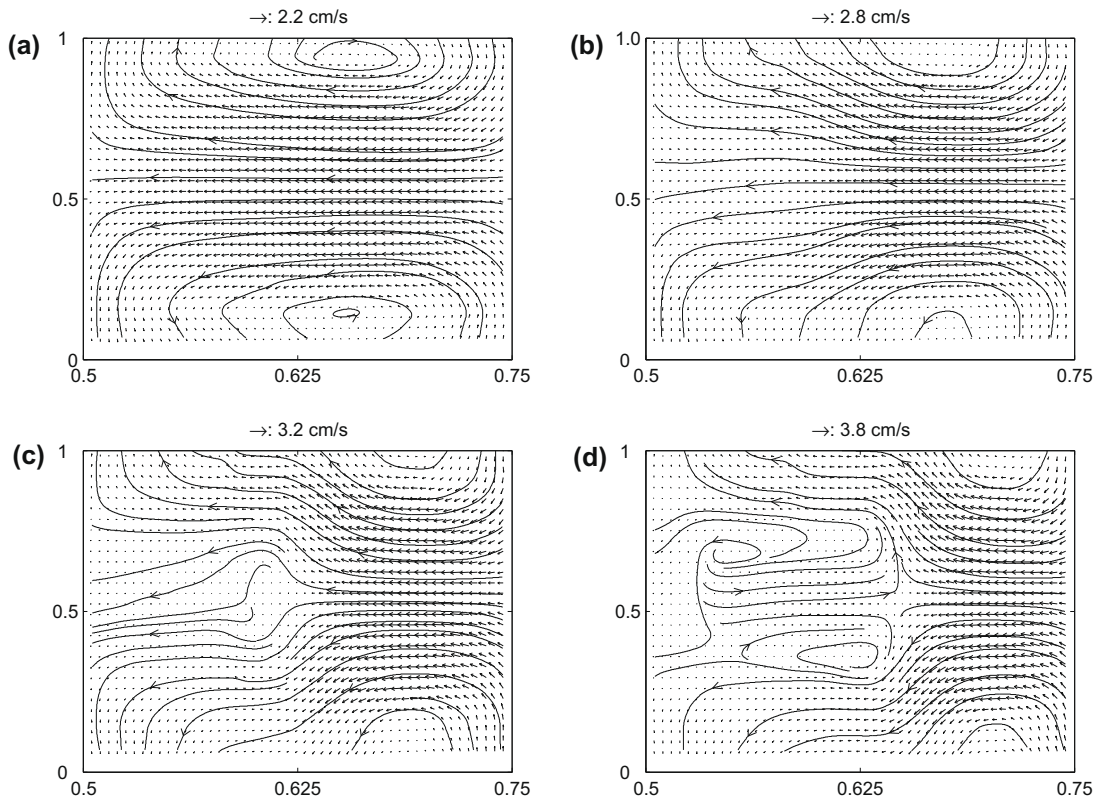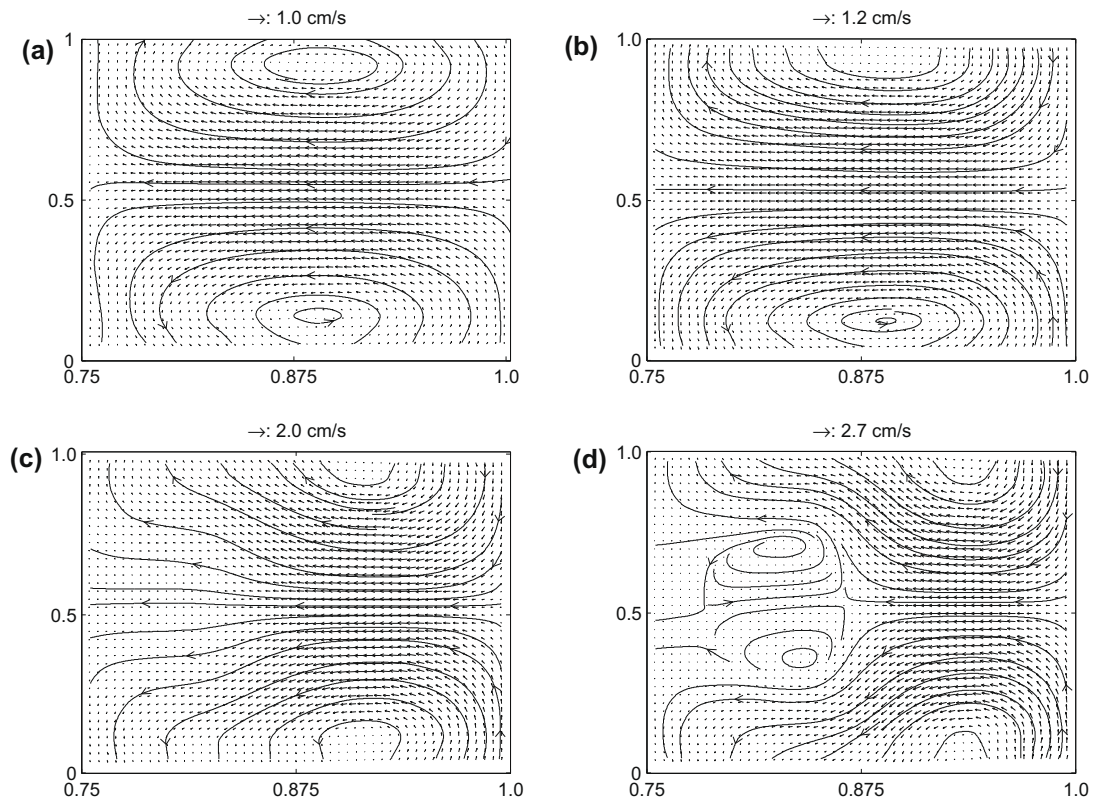

Fig. 4. The streaming flow structures in the half-wavelength region for (a) case A-5, (b) case A-6, (c) case A-7 and (d) case A-8.The horizontal axes are x/λ and the vertical axes are y/H. Note that the resolution of the velocity vectors was reduced to half in the plot for better visualization.

Fig. 5. The streaming flow structures in the quarter-wavelength region for (a) case B-5, (b) case B-6, (c) case B-7 and (d) case B-8. The horizontal axes are x/λ and the vertical axes are y/H. Note that the resolution of the velocity vectors was reduced to half in the plot for better visualization.

are generated in quarter of the wavelength near the channel centerline, which indicates that the flow patterns are clearly irregular.

The final set of experiments is conducted at the driver frequency of 1310 Hz ($T = 0.76$ ms) which allows the formation of four complete standing waves inside the channel. Four cases are considered in this set (cases C-1–C-4) that correspond to $X_{max} = 80$ μm, 102 μm, 145 μm and 190 μm, respectively. The corresponding maximum pressure amplitudes at pressure anti-node (P_0) are 1094, 1500, 2281 and 2716 Pa. The camera field of view is set equal to 13.1 cm in horizontal and 9.8 cm in vertical that allows to capture the streaming velocity field in half-wavelength region. The separation time between two PIV images of the image pair is set equal to 40 times the wave period (i.e. $\delta t = 30.5$ ms).

The time-averaged streaming velocity fields for cases C-1–C-4 are shown in Fig. 6. The plots show that for cases C-1 and C-2, the classical streaming patterns are observed i.e. four vortices per half-wavelength of the standing wave which are symmetric about the channel center line. Whereas, for cases C-3 and C-4, the streaming flow patterns are clearly irregular.

The difference between the regular and irregular streaming patterns can also be examined by comparing the experimental results with the theoretical streaming velocity which is valid for slow streaming. The variation of theoretical and experimental root-mean-square (RMS) of $u_{st}(u_{strms})$ with respect to the axial coordinate x for cases A-1 ($Re_{s2} = 16.1$, regular streaming) and A-4 ($Re_{s2} = 149.7$, irregular streaming) are plotted in Fig. 7a for comparison. The variation of theoretical and experimental values of u_{st} with respect to the transverse coordinate y for cases A-1 and A-4 at three axial positions ($x = \ell/4$, $\ell/2$, and $3\ell/4$) are shown in Fig. 7c and d. For the classical streaming case (left-hand side plots of Fig. 7), the shape of experimental results is similar to that of the theoretical ones which confirms the presence of regular streaming patterns. However, the maximum amplitudes of the experimental velocities are lower than the theoretical ones. This is due to this fact that the theoretical values are valid only for slow streaming ($Re_{s2} < 1$), whereas, for case A-1, $Re_{s2} = 16.1$. Thompson et al. [13] used LDA to measure u_{strms} with respect to x, and u_{st} with respect to y in a resonator with isothermal boundary condition for $Re_{s2} = 4, 10, 20$ and 40. They have also observed that as the streaming Reynolds number increases, the experimental acoustic velocities get smaller than the theoretical ones. It is also observed in left pane of Fig. 7c and d that for case A-1, the amplitudes of the experimental u_{st} close to the top and the bottom walls are not in agreement with the theoretical ones. The reason is that the field of view of the camera is set to cover the whole quarter-wavelength (10.3 cm). Therefore, The resolution of PIV velocity vectors for this case is not high enough to resolve the near wall region velocities.

For the irregular streaming case (case A-4, $Re_{s2} = 149.7$, right pane of Fig. 7), the shape of experimental velocities with respect to x and y are significantly deviated from that of the theoretical ones which confirms the presence of irregular
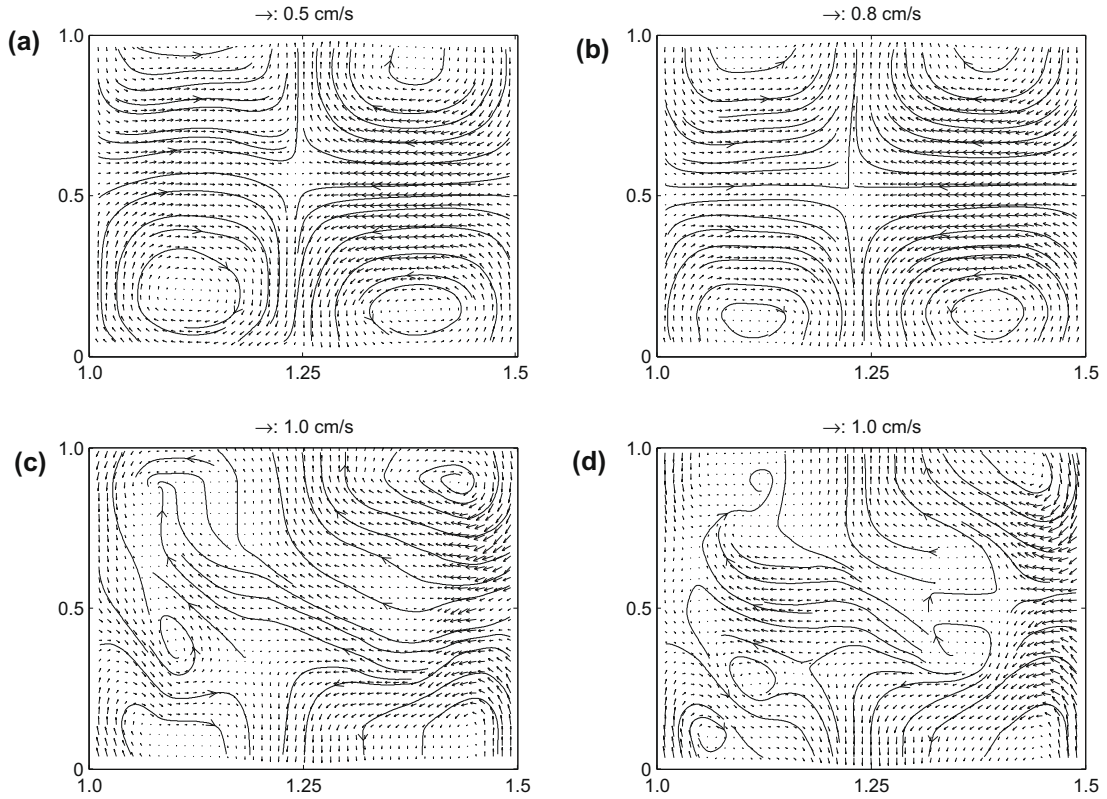
Fig. 6. The streaming flow structures in the quarter-wavelength region for (a) case C-5, (b) case C-6, (c) case C-7 and (d) case C-8. The horizontal axes are x/λ and the vertical axes are y/H. Note that the resolution of the velocity vectors was reduced to half in the plot for better visualization.

streaming patterns. According to Fig. 7, the peak of u_{strms} with respect to x is shifted away from the typical location (see Fig. 4a and b), and the experimental values of u_{st} with respect to y tend to zero in the center of the the channel. Negative amplitudes of u_{st} with respect to y are observed at $x = \ell/4$ (see right pane of Fig. 7b). This is due to existence of two additional small vortices at this location (see Fig. 4d). In addition to shape, the amplitudes of the axial streaming velocities are much lower than the theoretical ones. Linear theory (Eq. 1) predicts 8.2 cm/s for the maximum of u_{strms} with respect to x and 9 cm/s, 12.5 cm/s and 9 cm/s for the the maximum of u_{st} with respect to y at $x = \ell/4$, $\ell/2$, and $3\ell/4$, respectively, which are far larger than the measured values. This behavior can not be explained by the linear theory of acoustic streaming.

Different experimentally measured parameters for the cases studied, along with the remarks that whether the regular or irregular streaming is observed for the corresponding cases, are presented in Table 2. Using the results summarized in Table 2, we can classify regular and irregular streaming flow patterns based on the normalized channel width (H/ℓ) and the normalized maximum vibrational displacement (X_{max}/ℓ). The cases studied in terms of the normalized channel width (related to the vibrational frequency) versus the normalized maximum vibrational displacement (related to both vibrational displacement and frequency) are plotted in Fig. 8. The figure clearly shows that both vibrational amplitude and frequency affect the classical streaming structure. Using their numerical models, Kawahashi and Arakawa [7] and Aktas and Farouk [9] also found that the streaming structure can be affected by the vibrational amplitude and frequency. Fig. 8 also shows that as H/ℓ increases, the transition from regular to irregular streaming occurs at lower values of X_{max}/ℓ. It is also observed that the relationship between H/ℓ and X_{max}/ℓ at which the transition occurs is non-linear. We have attempted to establish this relationship through best fit to the data points of the lower bound where the irregular streaming patterns form. The relationship is found to be $X_{max}/\ell = a(H/\ell)^2 + b(H/\ell) + c$, where $a = 0.0739$, $b = -0.0425$, and $c = 0.0072$ (dashed line in Fig. 8). Since this equation is based on three data points which is the minimum number of data points to establish non-linear equation, more future experiments at different frequencies and amplitudes are needed to confirm the validity of this equation.

In the following, we have attempted to generalize the results obtained in the present study in terms of a dimensionless parameter. The values of Re_a (Eq. 2) and Re_{s1} (Eq. 3) for all given cases are presented in Table 2. The results show that Re_a and Re_{s1} are not appropriate to classify the streaming flow patterns. Using their numerical simulation, Aktas and Farouk [9] also found that the regular and irregular streaming patterns cannot be classified based on Re_a and Re_{s1} which is consistent with the present experimental results.

The values of Re_{s2} (Eq. 4) for all cases are also presented in Table 2. The results show that for cases A-1–A-4 ($f = 976$ Hz), the irregular streaming is observed at $Re_{s2} \geqslant 64$. At $f = 666$ Hz (cases B-1–B-4) the irregular streaming is observed at
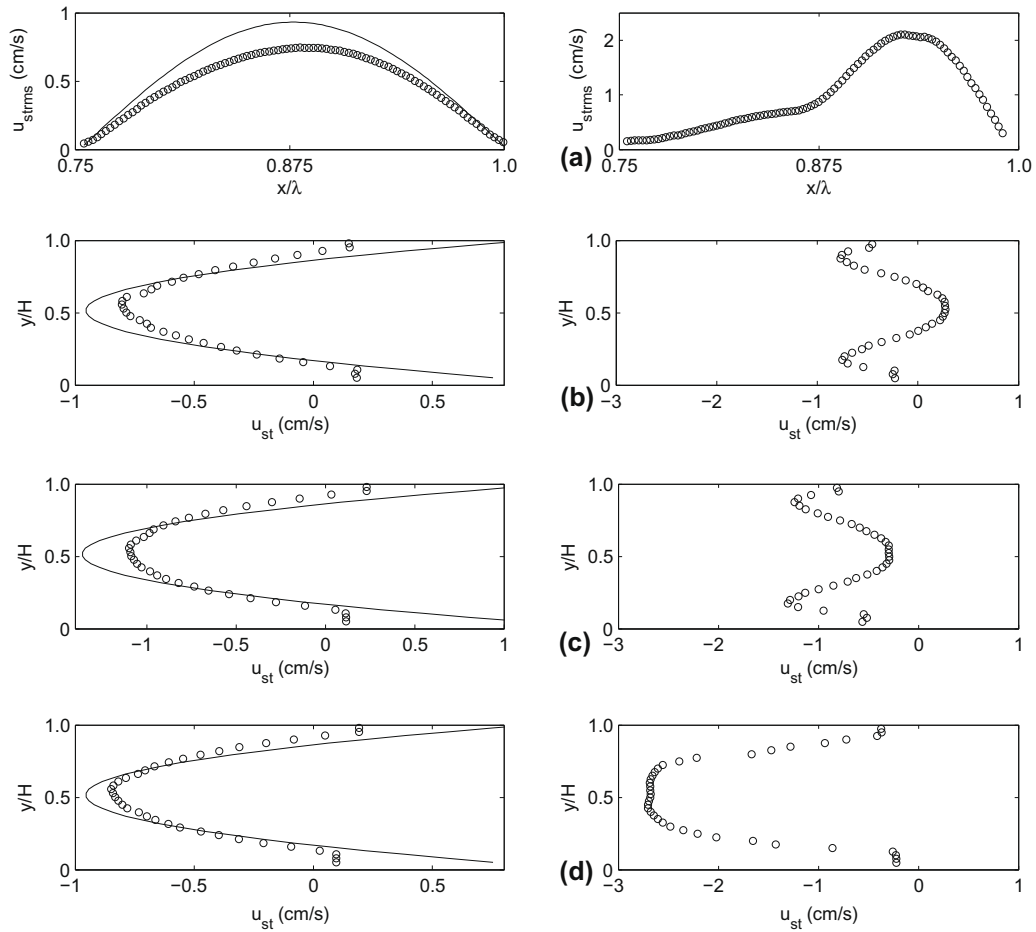
Fig. 7. (a) The variation of theoretical (solid line) and experimental (○) root-mean-square (RMS) of u_{st} (u_{strms}) with respect to the axial coordinate x. The variation of theoretical and experimental values of u_{st} with respect to the transverse coordinate y for cases B-5 ($Re_{s2} = 16.1$, regular streaming), left-hand side; and case B-8 ($Re_{s2} = 149.7$, irregular streaming), right-hand side, at three axial positions (b) $x = \ell/4$, (c) $x = \ell/2$ and (d) $x = 3\ell/4$.

Table 2
Different experimentally obtained parameters for the cases studied. P_0, maximum pressure; u_{max}, maximum acoustic velocity; u_{stmax}, maximum streaming velocity; Re_a, acoustic Reynolds number; Re_{s1} and Re_{s2}, streaming Reynolds numbers.

Case	P_0 (Pa)	u_{max} (m/s)	u_{stmax} (cm/s)	Re_a	Re_{s1}	Re_{s2}	Streaming pattern
A-1	1437	3.48	1.1	12514	127	16.1	Regular
A-2	1780	4.31	1.2	15498	194	24.7	Regular
A-3	2844	7.41	2.1	24692	496	64.1	Irregular
A-4	4375	10.6	2.7	38116	1174	149.7	Irregular
B-1	2469	5.98	2.2	31512	548	32.5	Regular
B-2	3094	7.49	2.8	39470	861	51.0	Irregular
B-3	3844	9.31	3.2	49060	1328	78.6	Irregular
B-4	4844	11.74	3.7	61856	2109	124.8	Irregular
C-1	1094	2.66	0.45	7126	54	12.6	Regular
C-2	1500	3.63	0.80	9425	104	23.6	Regular
C-3	2281	5.53	0.95	14815	238	54.4	Irregular
C-4	2716	6.58	1.0	17628	337	77.2	Irregular

$Re_{s2} \geqslant 51$, whereas at $f = 1310$ Hz (cases C-1–C-4), it is observed at $Re_{s2} \geqslant 54$. Therefore, it is inferred that whereas, Re_a and Re_{s1} are not appropriate parameters to classify the regular and irregular streaming patterns, Re_{s2} can be used for this purpose. Using their numerical model, Menguy and Gilbert [8] also predicted that the non-linear effect is controlled by the dimensionless number Re_{s2}. They argued that as Re_{s2} increases, the axial streaming velocity is distorted due to the inertia effect. Thompson et al. [13] measured streaming velocities for $f = 310$ Hz for isothermal boundary condition using LDA. They observed
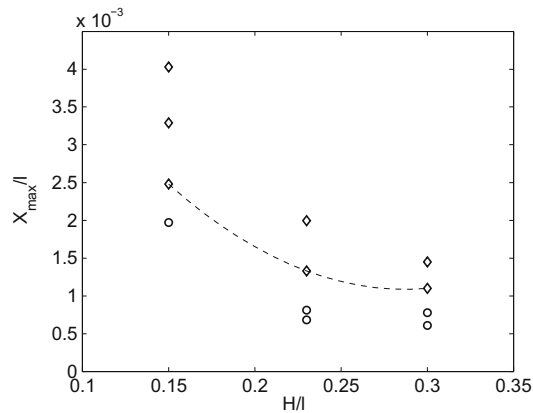
Fig. 8. The normalized channel width (H/ℓ) versus the normalized maximum vibrational displacement (X_{max}/ℓ) for all cases; ○, regular streaming structures; ◇, irregular streaming structures.

classical streaming behavior for and $4 < Re_{s2} < 40$. The results of these numerical and experimental studies are consistent with our experimental findings. Based on the results summarized in Table 2, it can be concluded that the irregular streaming patterns are observed at $Re_{s2} > 50$.

6. Conclusions

Experimental investigation of the formation of regular and irregular acoustic streaming velocity fields in an air-filled rigid-walled square channel subject to acoustic standing waves are performed using synchronized PIV technique. The resonator has been put inside a large water tank in order to maintain isothermal boundary conditions at the channel walls. The effects of the frequency and maximum vibrational displacement of the acoustic driver on the streaming structure are studied. The results show that for a given vibrational frequency, classical streaming structures are observed only when the vibrational displacement of the acoustic driver is not too large. A significant correlation is observed between the formation of regular and irregular streaming flow patterns and the frequency and vibrational displacement of the acoustic driver. The results also show that for the generation of irregular streaming flow patterns, Re_{s2} should be greater than 50.

Acknowledgements

References

[1] E.W. Haddon, N. Riley, A note on the mean circulation in standing waves, Wave Motion 5 (1983) 43–48.
[2] S. Boluriaan, P.J. Morris, Acoustic streaming: from Rayleigh to today, Int. J. Aeroacoust. 2 (2003) 255–292.
[3] F. Coulouvrat, A quasi-analytical shock solution for general nonlinear progressive waves, Wave Motion 46 (2009) 97–107.
[4] M. Nabavi, M.H.K. Siddiqui, J. Dargahi, A fourth-order accurate scheme for solving highly nonlinear standing wave equation in different thermoviscous fluids, J. Comput. Acoust. 16 (2008) 563–576.
[5] A. Kildal, Linear and non-linear fluid motion generated by an oscillating obstacle, Wave Motion 19 (1994) 171–187.
[6] F. Carlsson, M. Sen, L. Löfdahl, Steady streaming due to vibrating walls, Phys. Fluids 16 (2004) 1822–1825.
[7] M. Kawahashi, M. Arakawa, Nonlinear phenomena induced by finite amplitude oscillation of air-column in closed duct, JSME 39 (1996) 280–286.
[8] L. Menguy, J. Gilbert, Nonlinear acoustic streaming accompanying a plane stationary wave in a guide, Acustica 86 (2000) 249–259.
[9] M.K. Aktas, B. Farouk, Numerical simulation of acoustic streaming generated by finite-amplitude resonant oscillations in an enclosure, J. Acoust. Soc. Am. 116 (2004) 2822–2831.
[10] M.P. Arroyo, C.A. Greated, Stereoscopic particle image velocimetry, Measure. Sci. Technol. 2 (1991) 1181–1186.
[11] D.B. Hann, C.A. Greated, The measurement of flow velocity and acoustic particle velocity using particle image velocimetry, Measure. Sci. Technol. 8 (1997) 1517–1522.
[12] M.W. Thompson, A.A. Atchley, Simultaneous measurement of acoustic and streaming velocities in a standing wave using lase Doppler anemometry, J. Acoust. Soc. Am. 117 (2005) 1828–1838.
[13] M.W. Thompson, A.A. Atchley, M.J. Maccarone, Influences of a temperature gradient and fluid inertia on acoustic streaming in a standing wave, J. Acoust. Soc. Am. 117 (2005) 1839–1849.
[14] S. Moreau, H. Bailliet, J.C. Valiere, Measurements of inner and outer streaming vortices in a standing waveguide using lase Doppler anemometry, J. Acoust. Soc. Am. 123 (2008) 640–647.
[15] M. Nabavi, M.H.K. Siddiqui, J. Dargahi, Simultaneous measurement of acoustic and streaming velocities using synchronized PIV technique, Measure. Sci. Technol. 123 (2007) 1811–1817.
[16] M. Nabavi, M.H.K. Siddiqui, J. Dargahi, Measurement of the acoustic velocity field of nonlinear standing wave using the synchronized PIV technique, Exp. Therm. Fluid Sci. 33 (2008) 123–131.
[17] M. Nabavi, M.H.K. Siddiqui, J. Dargahi, Experimental investigation of the formation of acoustic streaming in a rectangular enclosure using the synchronized PIV technique, Measure. Sci. Technol. 19 (2008) 065405.

[18] M. Nabavi, M.H.K. Siddiqui, J. Dargahi, Influence of differentially heated horizontal walls on the streaming shape and velocity in a standing wave resonator, Int. Commun. Heat Mass Transfer 35 (2008) 1061–1064.
[19] M. Nabavi, M.H.K. Siddiqui, J. Dargahi, Analysis of the flow structure inside the valveless standing wave pump, Phys. Fluids 20 (2008) 126101.
[20] N. Rott, The influence of heat conduction on acoustic streaming, J. Appl. Math. Phys. 25 (1974) 417–421.
[21] W.H. Snyder, J.L. Lumley, Some measurements of particle velocity autocorrelation functions in a turbulent flow, J. Fluid Mech. 48 (1971) 41–71.
[22] D.A. Siegel, A.J. Plueddemann, The motion of a solid sphere in an oscillating flow: an evaluation of remotely sensed Doppler velocity estimates in the sea, J. Atmos. Ocean. Technol. 8 (1991) 296–304.
[23] M.H.K. Siddiqui, M.R. Loewen, C. Richardson, W.E. Asher, A.T. Jessup, Simultaneous particle image velocimetry and infrared imagery of microscale breaking waves, Phys. Fluids 13 (2001) 1891–1903.